Applied Research Laboratory

Technical Report

APPLICATION OF SMOOTHED PARTICLE
HYDRODYNAMICS TO FLUID FLOW
INVOLVING SOLID BOUNDARIES

by

C. S. McCormick
T. F. Miller

DISTRIBUTION STATEMENT A
Approved for public release
Distribution Unlimited

PENNSTATE

1855

DTIC QUALITY INSPECTED 1

The Pennsylvania State University
APPLIED RESEARCH LABORATORY
P.O. Box 30
State College, PA 16804

APPLICATION OF SMOOTHED PARTICLE HYDRODYNAMICS TO FLUID FLOW INVOLVING SOLID BOUNDARIES

by

C. S. McCormick
T. F. Miller

Technical Report No. TR 96-006
June 1996

Supported by:
Space and Naval Warfare Systems Command

L.R. Hettche, Director
Applied Research Laboratory

Approved for public release; distribution unlimited

19960628 040

REPORT DOCUMENTATION PAGE

Form Approved
OMB No. 0704-0188

Public reporting burden for this collection of information is estimated to average 1 hour per response, including the time for reviewing instructions, searching existing data sources, gathering and maintaining the data needed, and completing and reviewing the collection of information. Send comments regarding this burden estimate or any other aspect of this collection of information, including suggestions for reducing this burden, to Washington Headquarters Services, Directorate for Information Operations and Reports, 1215 Jefferson Davis Highway, Suite 1204, Arlington, VA 22202-4302, and to the Office of Management and Budget, Paperwork Reduction Project (0704-0188), Washington, DC 20503.

1. AGENCY USE ONLY (Leave blank)

2. REPORT DATE
April 1994

3. REPORT TYPE AND DATES COVERED
Undergraduate Honors Thesis

4. TITLE AND SUBTITLE
Application of Smoothed Particle Hydrodynamics to Fluid Flow Involving Solid Boundaries

5. FUNDING NUMBERS
1999

6. AUTHOR(S)
C. S. McCormick
T. F. Miller

7. PERFORMING ORGANIZATION NAME(S) AND ADDRESS(ES)
Applied Research Laboratory
The Pennsylvania State University
P. O. Box 30
State College, PA 16804

8. PERFORMING ORGANIZATION REPORT NUMBER
TR#96-006

9. SPONSORING/MONITORING AGENCY NAME(S) AND ADDRESS(ES)
Space and Naval Warfare Systems Command
Code OOL
2451 Crystal Drive
Arlington, VA 22202

10. SPONSORING/MONITORING AGENCY REPORT NUMBER

11. SUPPLEMENTARY NOTES

12a. DISTRIBUTION/AVAILABILITY STATEMENT

12b. DISTRIBUTION CODE

13. ABSTRACT (Maximum 200 words)
Smoothed particle hydrodynamics (SPH) is a non-Monte Carlo free-Lagrangian method of computational fluid dynamics that has recently expanded in scope beyond its parent application of astrophysical simulations. Modelling terrestrial flows involving boundaries is an important extension of the technique. This thesis describes the application of SPH to model compressible and incompressible flows involving boundaries.

Simulations of shock wave reflection in a one-dimensional shock tube have been made. Different boundary methods have been compared with regards to their ability to model a one-dimensional reflecting shock wave. The simulations show that the introduction of imaginary particles appears to be the most effective method of boundary simulation for transient shock reflection. Simulations also show that the choice of artificial diffusion treatment for best reflection is ambiguous.

Incompressible flow has beenmodelled using several test problems. To model incompressible flow, modifications to the standard SPH equations are necessary. An artificial compressibility technique is introduced through a fluid specific equation of state. Real viscisity has been introduced. Results are shown for three test cases: Couette flow, Stoke's first problem, and a shear driven cavity.

14. SUBJECT TERMS
Smoothed Particle Hydrodynamics, SPH, CFD, Lagrangian Fluid Dynamics

15. NUMBER OF PAGES
39

16. PRICE CODE

17. SECURITY CLASSIFICATION OF REPORT
UNCLASSIFIED

18. SECURITY CLASSIFICATION OF THIS PAGE
UNCLASSIFIED

19. SECURITY CLASSIFICATION OF ABSTRACT
UNCLASSIFIED

20. LIMITATION OF ABSTRACT

ABSTRACT

Smoothed particle hydrodynamics (SPH) is a non-Monte Carlo free-Lagrangian method of computational fluid dynamics that has recently expanded in scope beyond its parent application of astrophysical simulations. Modelling terrestrial flows involving boundaries is an important extension of the technique. This thesis describes the application of SPH to model both compressible and incompressible flows involving boundaries.

Simulations of shock wave reflection in a one-dimensional shock tube have been made. Different boundary methods have been compared with regards to their ability to model a one-dimensional reflecting shock wave. The simulations show that the introduction of imaginary particles appears to be the most effective method of boundary simulation for transient shock reflection. Simulations also show that the choice of artificial diffusion treatment for best reflection is ambiguous.

Incompressible flow has been modeled using several test problems. To model incompressible flow, modifications to the standard SPH equations are necessary. An artificial compressibility technique is introduced through a fluid specific equation of state. Real viscosity has been introduced. Results are shown for three test cases: Couette flow, Stoke's first problem, and a shear driven cavity.

TABLE OF CONTENTS

ABSTRACT ii

LIST OF FIGURES iv

NOMENCLATURE v

Chapter 1: INTRODUCTION 1

Chapter 2: FUNDAMENTALS 3

2.1 Theory 3
2.2 Equations of Motion 4
2.2.1 Mass Conservation 4
2.2.2 Momentum Equation 5
2.2.3 Internal Energy Equation 5
2.3 Kernels 6
2.4 Artificial Diffusion 7
2.4.1 Monaghan-Gingold artificial viscosity 8
2.4.2 Flux corrected transport 8
2.5 Time Stepping 9
2.6 Boundary Conditions 10

Chapter 3: COMPRESSIBLE FLOW 13

3.1 The Test Problem 13
3.2 Discussion 13
3.2.1 Pre-reflection 13
3.2.2 Artificial diffusion 15
3.2.3 Reflected shock 17
3.3 Conclusion 24

Chapter 4: INCOMPRESSIBLE FLOW 25

4.1 Introduction 25
4.2 Modifications 25
4.2.1 Artificial compressibility 26
4.2.2 Viscous term 26
4.3 Boundary Treatment 27
4.4 The Test Problems 28
4.5 Discussion 29
4.6 Conclusions 36

Chapter 5: CONCLUSION/RECOMMENDATIONS 37

REFERENCES 38

LIST OF FIGURES

Figure 1: Plots of a) velocity, b) pressure, c) density, and d) temperature 0.9 milliseconds into the simulation, but before reflection. The simulation uses Monaghan-Gingold artificial viscosity (dashed line), and is compared to the exact solution (solid line).

Figure 2: Plots of a) velocity, b) pressure, c) density, and d) temperature 0.9 milliseconds into the simulation, but before reflection. The simulation uses flux corrected transport (dashed line), and is compared to the exact solution (solid line).

Figure 3: Comparison of pre-reflection shock wave simulations using M-G (fine-dashed line), and FCT (coarse-dashed line) for artificial diffusion. Exact solution is the solid line.

Figure 4: Plots of a) velocity, b) pressure, c) density, and d) temperature 1.65 milliseconds into the simulation, and after reflection. Simulation uses Monaghan-Gingold artificial viscosity (dashed line), and the imaginary particle boundary treatment.

Figure 5: Plots of a) velocity, b) pressure, c) density, and d) temperature 1.65 milliseconds into the simulation, and after reflection. Simulation uses flux corrected transport (dashed line), and the imaginary particle boundary treatment.

Figure 6: Plots of a) velocity, b) pressure, c) density, and d) temperature 1.65 milliseconds into the simulation, and after reflection. Simulation uses Monaghan-Gingold artificial viscosity (dashed line), and the repulsive force (spring) boundary treatment.

Figure 7: Plots of a) velocity, b) pressure, c) density, and d) temperature 1.65 milliseconds into the simulation, and after reflection. Simulation uses flux corrected transport (dashed line), and the repulsive force (spring) boundary treatment.

Figure 8: Plot of the fully developed velocity profile for Couette flow.

Figure 9: Plot of transient velocity profile for Stoke's first problem at 0.001 seconds (dashed line).

Figure 10: Particle streaklines at 120.0 seconds for a Reynold's number of 10

Figure 11: Particle distribution at 120.0 seconds for the driven cavity with a Reynold's number of 10.

Figure 12: Velocity profile along vertical centerline for the driven cavity with a Reynold's number of 10.

Figure 13: Velocity profile along horizontal centerline for Reynold's number of 10.

NOMENCLATURE

c_{ij}	=	Local speed of sound
$F(r)$	=	Arbitrary function
f^d	=	Diffusive flux
f^{ad}	=	Anti-diffusive flux
h	=	Smoothing length
i	=	Subscript defining individual particle
j	=	Subscript defining a summation index
m	=	Mass
n	=	Number of particles
P	=	Pressure
q	=	General variable
R_b	=	Boundary position
r	=	Position
r_{ij}	=	Distance between particles
t	=	Time
u	=	Internal energy
v	=	Velocity
W_{ij}	=	Weighting kernel
B	=	Water equation of state constant
α, β, η	=	Artificial viscosity constants
δ	=	Dirac delta function
Π	=	Artificial viscosity
Π'	=	Viscous stress
ρ	=	Density
ρ_o	=	Initial density
γ	=	Distance/smoothing length
χ	=	Relaxed force distance
κ	=	Force constant
μ	=	Diffusion coefficient for FCT
μ_{ij}	=	Monaghan's viscosity coefficient
Γ	=	Water equation of state exponent
ν	=	Antidiffusion coefficient for FCT
ν'	=	Kinematic viscosity

Chapter 1. INTRODUCTION

Smoothed particle hydrodynamics (SPH) is a free-Lagrangian computational method introduced by Lucy [1], and Gingold and Monaghan [2]. This method was originally developed for the simulation of such astrophysical phenomena as binary star interactions [3], super nova explosions [4], and the origin of the moon [5-7]. Recently, more interest has centered on the terrestrial applications of SPH. Libersky and Petschek [8] have adapted SPH to simulate high speed impacts of solid objects. Several authors [9-11] have simulated unsteady gas-dynamic shock tube problems. Henneken and Icke [12] have reproduced shock waves formed by steady supersonic flow impinging on a forward facing step. Other applications include the modeling of volcanic ash flows [13], and simple free surface incompressible flows [14].

The basic premise of SPH is to model a continuous fluid as a discrete collection of interacting particles. Each particle has characteristic properties of mass, velocity, position, and energy associated with it. These values are updated through a timestepping algorithm. Smoothed particle hydrodynamics does not need a mesh or finite differences to compute spatial derivatives. Derivatives are calculated through the use of a weighting kernel, with particles loosely viewed as interpolation points. The kernel is a smoothing function with a smoothing length set such that the effects of a central particle just reach its nearest neighbors. By use of a kernel, the mesh-tangling problems of grid-based Lagrangian codes are avoided.

Smoothed particle methods differ from Monte-Carlo methods because they do not use random number generation to determine the outcome of particle collisions or diffusion. A benefit that SPH has in common with other explicit Lagrangian methods is that it is naturally suited for massively parallel computation. An individual processor can be assigned to an individual particle. As massively parallel machines become larger and more commonly used, this advantage should promote wider use of SPH.

The primary objective of this thesis is to expand and evaluate SPH for situations involving solid boundaries. Because astrophysical phenomena typically have no solid boundaries, this area has received little attention.

The next chapter of this thesis introduces the SPH technique. The third chapter reviews work on modeling compressible flows involving boundaries. Reflected shock waves in a one-dimensional shock tube have been simulated. Several different schemes have been considered for simulating the presence of solid reflective boundaries. The effects of an alternative artificial diffusion treatment have also been examined. The fourth chapter reviews work in extending SPH to model incompressible flow. This requires the use of an artificial compressibility technique. Real viscosity has been added to the equations of motion and a driven cavity has been simulated. The final chapter concludes the thesis and make recommendations for further study.

Chapter 2. FUNDAMENTALS

2.1 Theory

Smoothed particle hydrodynamics treats a fluid as a collection of particles; each having its own characteristic properties of velocity, energy, and mass. Any function, F(r), can then be estimated using an integral interpolant, with the particles acting as interpolation points:

$$\langle F(r)\rangle = \int F(r')W(r-r',h)dr' \tag{1}$$

with W(r-r',h) being the interpolation kernel (hereafter abbreviated as W_{ij}). If the particles are distributed in the domain with a number density n(r), then Equation (1) can be approximated by

$$\langle F(r)\rangle = \Sigma\ F_j/n_j * W_{ij}. \tag{2}$$

Here the summation is taken over all particles. The number density can then be represented by use of the particles' characteristic mass and density by

$$n(r_j) = \rho(r_j)/m_j. \tag{3}$$

Thus Equation (2) can be written as

$$\langle F(r)\rangle = \Sigma\ F_j m_j/\rho_j * W_{ij}. \tag{4}$$

The equations of motion may be derived from this basic relation.

2.2 Equations of Motion

2.2.1 Mass conservation

Mass conservation is satisfied by direct substitution of ρ for F in Equation (4):

$$\rho_i = \Sigma\rho_j m_j/\rho_j * W_{ij} \tag{5}$$

or

$$\rho_i = \Sigma m_j W_{ij}. \tag{6}$$

An alternative approach for determining ρ is through use of the Eulerian continuity equation:

$$\partial\rho/\partial t + \rho\nabla\cdot v = 0. \tag{7}$$

The product of density and the velocity divergence is

$$(\rho\nabla\cdot v)_i = \nabla_i\cdot(\rho_i v_i) - v_i\nabla_i\rho_i. \tag{8}$$

Applying Equation (4) yields

$$(\rho\nabla\cdot v)_i = \Sigma(\rho v)_j m_j/\rho_j\ \nabla_i W_{ij} - \Sigma v_i\rho_j m_j/\rho_j\ \nabla_i W_{ij}. \tag{9}$$

Reducing gives the following form for the divergence term

$$(\rho\nabla\cdot v)_i = \Sigma(v_j - v_i) m_j \nabla_i W_{ij}. \tag{10}$$

The density can now be calculated from:

$$d\rho_i/dt = -\Sigma m_j(v_i - v_j)\cdot\nabla_i W_{ij}. \tag{11}$$

With this method the density will only change when particles move relative to one another. The advantage of using the divergence form (Eq. 11) in preference to the mass summation form (Eq. 6) manifests as a savings in CPU time. All the subsequent governing equations can be solved using only the divergence of the kernel; the kernel itself needs not be calculated. A disadvantage of the divergence form is that mass is not strictly conserved [15].

2.2.2 Momentum equation

The momentum equation for an inviscid fluid without body fórces is

$$dv/dt = -1/\rho * \nabla P. \tag{12}$$

It is advantageous to write this equation in its symmetric form, so that linear and angular momentum are conserved exactly [15]. Thus, we write

$$dv/dt = -\nabla(P/\rho) - (P/\rho^2)\nabla\rho. \tag{13}$$

Applying Equation (4) yields:

$$dv_i/dt = -[\Sigma(P_j/\rho_j)m_j/\rho_j\ \nabla W_{ij} + \Sigma(P_i/\rho_i^2)\rho_j m_j/\rho_j\ \nabla W_{ij}]. \tag{14}$$

Reducing and combining like terms gives the final form of the momentum equation.

$$dv_i/dt= -\Sigma m_j*(P_i/\rho_i^2 + P_j/\rho_j^2)\nabla_i W_{ij}. \tag{15}$$

2.2.3 Internal energy equation

The rate of change of internal energy is

$$du/dt = -(P/\rho)\nabla\cdot v. \tag{16}$$

In symmetric form this equation is:

$$du/dt = -\nabla\cdot(Pv/\rho) + v\cdot\nabla(P/\rho). \tag{17}$$

Applying Equation (4) to the energy equation yields:

$$du_i/dt = \Sigma m_j*(P_j/\rho_j^2)(v_i-v_j)\cdot\nabla_i W_{ij}. \tag{18}$$

2.3 Kernels

The kernel needs to satisfy two restrictions:

$$\int W(r-r',h)dr' = 1 \tag{19}$$

and

$$\lim_{h\to 0} W(r-r',h) = \delta(r-r'). \tag{20}$$

The kernel should also have continuous first and second derivatives. One obvious kernel is a gaussian curve; another is an exponential

$$W = 1/\pi^{3/2} \exp(-(r-r')^2/h^2) \tag{21}$$

where h is the smoothing length. This curve has the appearance of a gaussian and satisfies the above requirements (Eqs. 19 and 20). One problem with this form is that one particle interacts with all of the other particles in the domain (albeit extremely weakly with most). This causes CPU time requirements to scale with the square of the number of particles.

A more economical choice of a kernel is a weighting system that offers compact support. Compact support limits one particle's interactions to a definite surrounding volume. This allows the code to be written with linked lists by superimposing a grid over the particles which serves to locate neighboring particles. The grid needs not conform to the precise problem geometry, nor is any information stored at nodal locations; thus no grid entanglements are produced. The width of the grid cells is set such that a particle in one cell can only interact with particles in the immediately neighboring cells. This technique [17,18] allows CPU time to scale proportionally with the

number of particles. The compact kernel [19] used for this paper is defined by:

$$W(r,h) = \sigma/h^{\xi} \begin{cases} (1-1.5\gamma^2+.75\gamma^3)/(\pi h) & 0<\gamma<1 \\ (.25*(2-\gamma)^3)/(\pi h) & 1<\gamma<2 \\ 0 & \gamma>2 \end{cases} \qquad (22)$$

with γ = distance/smoothing length, ξ is the number of dimensions and σ is the normalization constant. In one, two, and three dimensions this constant is set to 2/3, $10/7\pi$, and $1/\pi$ respectively. The smoothing length, h, is generally taken to be twice the distance between particles.

Another problem with the exponential form is that information can propagate over the entire computational domain in a single time step. For application of SPH to problems involving supersonic flows, the kernel can introduce errors because downstream values should have no effect on the flow upstream of the shocks. In SPH the kernel allows particles both downstream and upstream to be used in calculating shock values. A compact support formulation of the kernel can help reduce the downstream influence.

2.4 Artificial Diffusion

Artificial diffusion is required to dampen nonphysical, high-frequency oscillations that are inherent to Lagrangian simulations. Previously, artificial diffusion has been implemented in SPH through various artificial viscosity formulations.

2.4.1 Monaghan-Gingold artificial viscosity

Monaghan and Gingold [9] have formed the most widely used form for artificial viscosity (hereafter described as M-G viscosity) which is implemented by rewriting the momentum equation as:

$$dv_i/dt = -\Sigma m_j*(P_i/\rho_i^2+P_j/\rho_j^2+\Pi_{ij})\nabla_i W_{ij}. \tag{23}$$

where

$$\Pi_{ij} = \begin{cases} -(\alpha c_{ij}\mu_{ij}+\beta\mu_{ij}^2)/\rho_{ij} & \text{if } v_{ij}\cdot r_{ij}>0 \\ 0 & \text{if } v_{ij}\cdot r_{ij}<0. \end{cases} \tag{24}$$

Here

$$\mu_{ij}= (hv_{ij}\cdot r_{ij})/(r_{ij}^2+\eta^2), \tag{25}$$

and c_{ij} is the local speed of sound. Artificial viscosity is introduced only when particles are approaching. The constants α,β, and η^2 are generally set equal to 1, 2, and $.01h^2$; respectively.

2.4.2 Flux corrected transport

An alternative implementation of artificial diffusion, previously unused in SPH simulations, is flux corrected transport [20] (FCT). Flux corrected transport is a two-step process in which diffusion is applied everywhere in the first (predictor) stage to eliminate high frequency oscillations, and anti-diffusion is selectively added near discontinuities in the second (corrector) stage to reduce smearing. The criteria for elimination is determined by the relative location of the particle with respect to steep gradients of density. The diffusion is applied on an individual particle basis and whenever a fluid quantity is added to at one point, it is subtracted from another. Therefore, there is no net gain or loss incurred on the system as a whole. The general algorithm, following Book et al. [21], is:

1. Generate diffusive fluxes:

$$f^{d}_{j+1/2} = \nu_{j+1/2}(q^{n}_{j+1}-q_{j}^{n})$$

2. Generate anti-diffusive fluxes:

$$f^{ad}_{j+1/2} = \mu_{j+1/2}(q^{**}_{j+1}-q^{**}_{j})$$

3. Diffuse solution:

$$q^{***}_{j} = q_{j}^{**}+f_{j+1/2}^{d}-f^{d}_{j-1/2}$$

4. Calculate first differences of q_j^{***}:

$$\Delta q^{***} = q_{j+1}^{**}-q_{j}^{***}$$

5. Limit antidiffusive fluxes:

$$S = \text{sign of } (f_{j+1/2}^{ad})$$

$$f_{j+1/2}^{ad} = S\ \max[0,\min\{S\Delta q_{j-1/2}^{***},\ |f_{j+1/2}^{ad}|,\ S\Delta q_{j+3/2}^{***}\}]$$

6. Antidiffuse solution:

$$q_{j}^{n+1} = q_{j}^{***}-f_{j+1/2}^{ad}+f_{j-1/2}^{ad}$$

The diffusion, ν, and antidiffusion, μ, coefficients are dependent on the computational scheme. For SPH, ν and μ were optimized to be 0.5 and 0.25 respectively.

2.5 Time Stepping

A second order Runge-Kutta scheme was used to march the transport equations in time. For simulations involving FCT the diffusion and anti-diffusion were calculated before and after the timestep (no calculations were made at the intermediate step). Because SPH is an explicit scheme, there is a stability constraint placed on the size of the time step. For the shock tube problem, Monaghan and Gingold [9] suggested a timestep limit of $\Delta t \leq 0.3h/c_i$, where c_i is the local speed

of sound for the particle. All simulations were run with a time step under this limit.

2.6 Boundary Conditions

The treatment of rigid boundaries has received relatively little attention in flow simulations using SPH. There are several potential schemes that might be considered for implementing a reflecting boundary: imaginary particles, repulsive forces, immobile particles, or boundary modifications to the equations of motion.

Libersky and Petschek [8] used imaginary particles to model the impact of an iron rod with a rigid surface. The imaginary particle scheme works by placing extra particles along the outside edge of the boundary. For every "real" particle within a distance 2h of the boundary, an extra particle is placed symmetrically on the opposite side of the boundary. These particles have the same density and pressure, and a velocity opposite that of their corresponding real particle counterpart.

Because the imaginary particles must be included in the computation, this technique requires extra CPU time and memory. Extension to multi-dimensional simulations may create particle tracking problems. Instead of carrying the extra particles through the summation, it is possible to implement the boundaries using a series of logical if-then statements. When a real particle come within a distance, 2h, of the boundary, a series of if-then steps can be used to determine if additional calculations need to be made. This eliminates

the need to keep track of imaginary particles, allowing for easier multi-dimensional coding, and reduced memory and CPU requirements.

Monaghan [14] has used the repulsive force technique for simple free-surface incompressible flow simulations. Nagasawa and Kuwahara [13] have used this technique for modeling volcanic ash flows as well. The repulsive force technique works by introducing an interparticle force between boundary particles and the approaching fluid particles. If a particle moves within a preset distance, a repulsive force is added to the momentum summation. This force can be modeled as a Lennard-Jones type intermolecular force [13,14]:

$$f(r) = \begin{cases} \kappa_{ij}((\chi/R_b)^4 - (\chi/R_b)^2)/R_b & \text{if } \chi<R_b \\ 0 & \text{if } \chi>R_b \end{cases} \tag{26}$$

where χ is usually set equal to the initial particle separation, R_b is the distance to the boundary, and κ_{ij} is determined by the initial conditions. Alternately, the repulsive force can be modeled by a simple spring force:

$$f(r) = \begin{cases} \kappa_s(\chi-R_b)^2 & \text{if } \chi<R_b \\ 0 & \text{if } \chi>R_b \end{cases} \tag{27}$$

where χ is the relaxed spring distance (taken to be the initial particle separation), and κ_s is the spring force constant which is determined by the initial conditions. Since this method does not involve extra particles, except for those used to outline the boundary, there are only modest memory requirements.

The immobile particle, or infinite inertia, boundary treatment involves placing stationary particles along the boundaries. These particles are included in the summations, and after each iteration their

velocities are reset to zero. This technique seems most applicable for inactive boundaries in which there are no new forces being applied to the boundary. Campbell [16] showed that in certain simulations where the boundary pressure is known, boundaries can be implemented by modification of the equations of motion. This technique works for problems involving a fluid being driven by an external force (such as piston type or bullet/gun barrel simulations).

Chapter 3. COMPRESSIBLE FLOW

3.1 The Test Problem

One of the vehicles for testing the boundary and artificial diffusion treatments is a close-ended, one-dimensional, adiabatic shock tube. This problem involves simulating the expansion and shock waves generated when a wall separating high and low pressure regions of a perfect gas is suddenly removed. Unlike previous SPH work with the shock tube problem, simulations were continued until after the shock wave reflected off the tube end-walls. Inviscid, one-dimensional theory provides an exact solution that is valid until the reflected wave impinges upon the following contact surface. The model shock tube is 1.2 meters long and has an initial pressure ratio of four to one. The SPH simulation used 450 particles with a width set equal to the twice the initial separation on the low density side. All simulations used the imaginary particle technique for the boundary on the rarefaction end of the tube.

3.2 Discussion

3.2.1 Pre-reflection

Figure 1 shows plots of density, pressure, temperature, and velocity in the model shock tube 0.9 milliseconds into the simulation, but before reflection. This simulation used the M-G form of artificial viscosity. The SPH simulation tracks the location and magnitude of the expansion and compression fronts well. Notable errors include the blip in the pressure plot, an overprediction in the velocity rarefaction

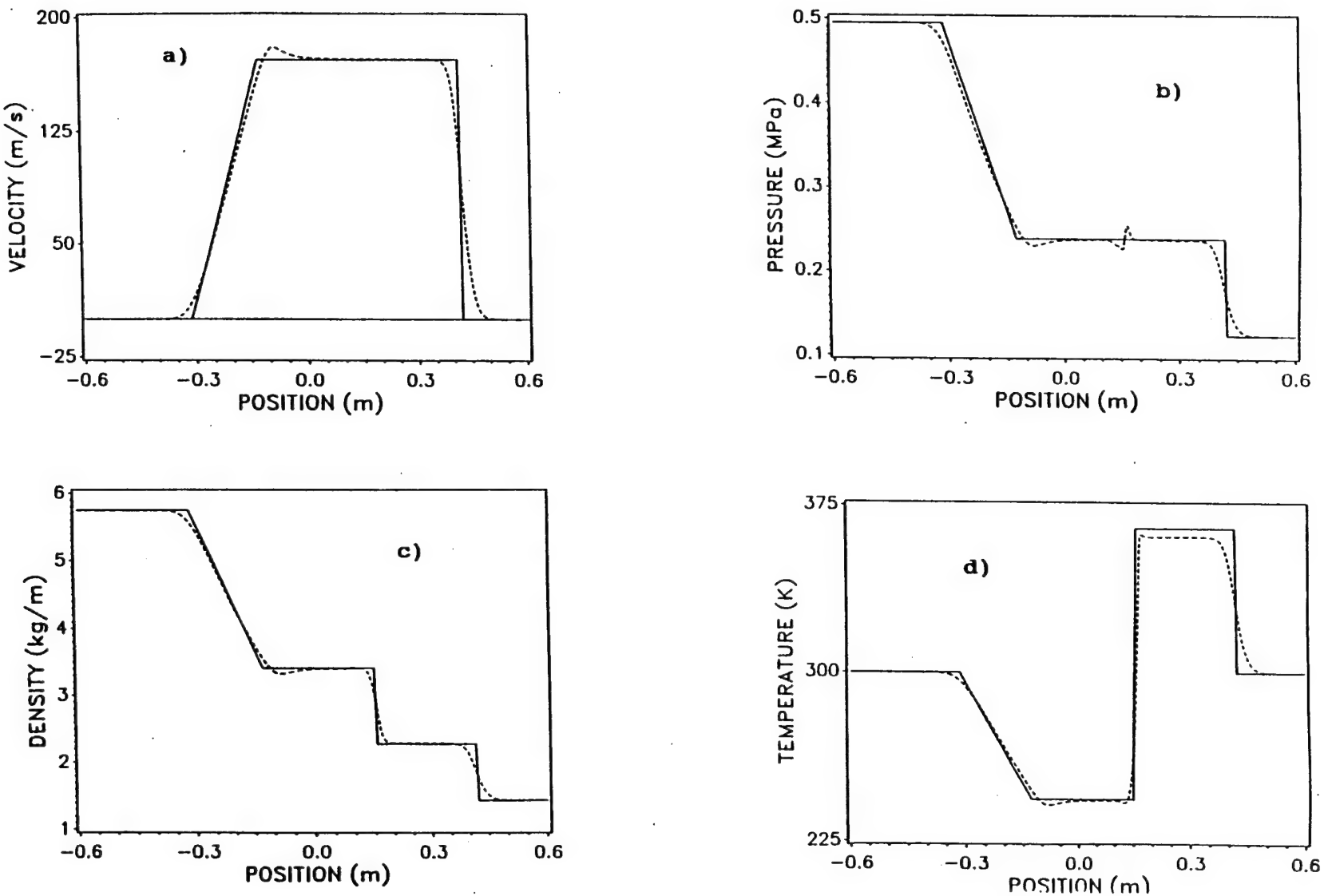

Figure 1: Plots of a) velocity, b) pressure, c) density, and d) temperature 0.9 milliseconds into the simulation, but before reflection. The simulation uses Monaghan-Gingold artificial viscosity (dashed line), and is compared to the exact solution (solid line).

wave, and smoothing of the shock wave fronts. Monaghan and Gingold [9] attribute the pressure blip to the influence of the contact discontinuity. The smoothing of the shock fronts (over a distance 3h) is due to the application of artificial diffusion. These results show that our simulation matches previous SPH work [9-11]. The simulation underpredicts the temperature immediately after the shock. Comparisons against other temperature predictions in the SPH literature cannot be made because these others were either run isothermally [11] or did not provide temperature results [9,10].

3.2.2 Artificial diffusion

The purpose of adding artificial diffusion is to damp out high frequency oscillations that form in the presence of flow discontinuities, like shock waves. While this is common practice in Eulerian simulations, the Lagrangian nature of SPH makes it even more necessary. Previous SPH shock tube work [9,11] has tested a variety of artificial viscosity forms, and concluded that the Monaghan-Gingold [9] (M-G) viscosity (used to produce the Figure 1 results) leads to the most accurate results for the adiabatic shock tube problem.

Figure 2 shows plots of the pre-impact shock waves using flux corrected transport (FCT). Comparison with Figure 1 shows that both artificial diffusion techniques prevent high frequency oscillations from forming. Flux corrected transport reduces the errors seen in the rarefaction overprediction and also reduces smoothing of the shock fronts.

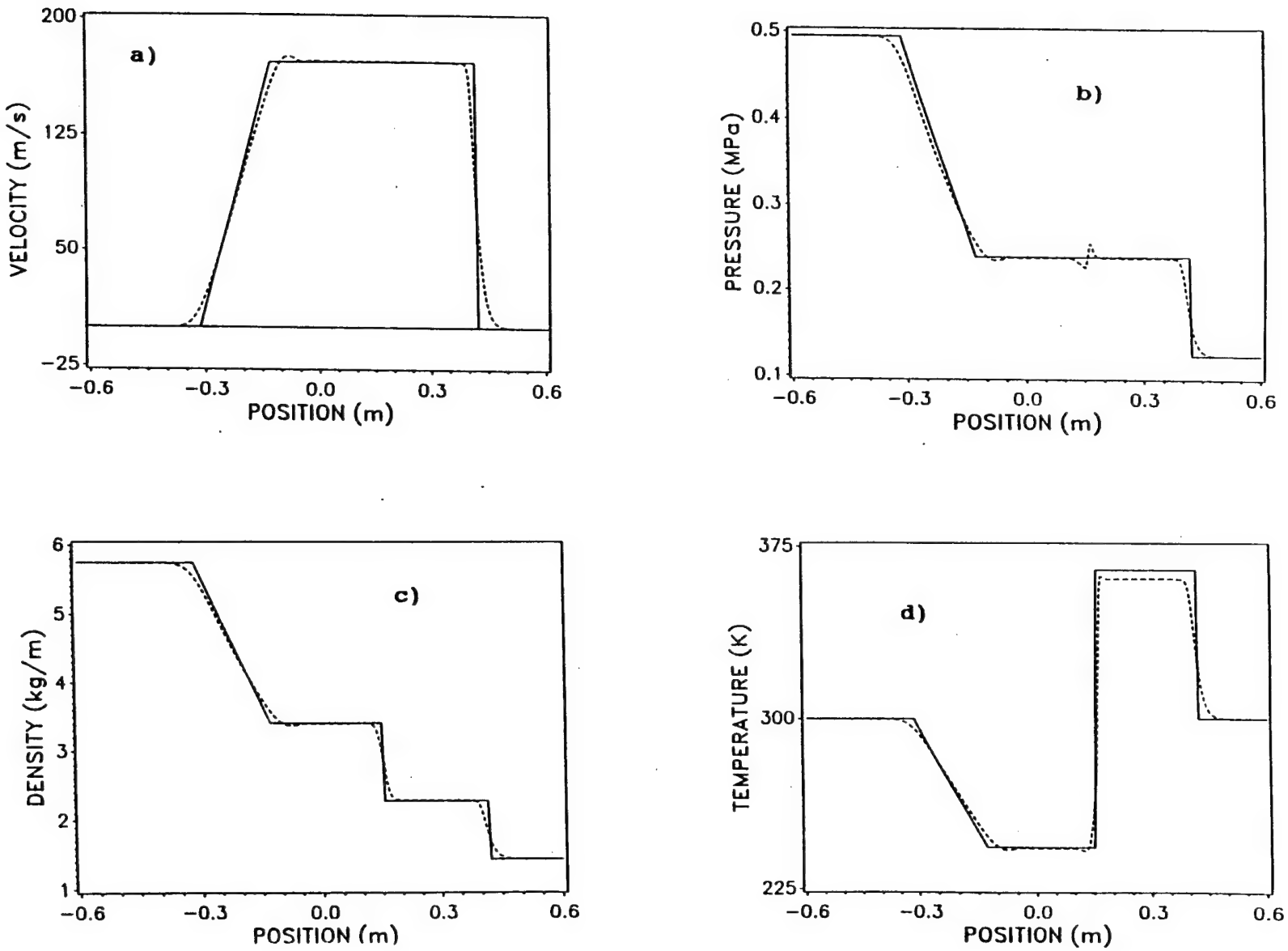

Figure 2: Plots of a) velocity, b) pressure, c) density, and d) temperature 0.9 milliseconds into the simulation, but before reflection. The simulation uses flux corrected transport (dashed line), and is compared to the exact solution (solid line).

Figure 3 shows the enlarged velocity profiles predicted using M-G viscosity and FCT, where FCT more accurately reproduces the shock front. Another criteria for comparison of the two artificial diffusion schemes is the CPU time required for calculations. An artificial viscosity treatment requires a summation over nearest neighbors, while FCT requires only a loop over the particles. Code using FCT ran approximately 15% faster than identical code using M-G viscosity.

3.2.3 Reflected shock

Four different end wall techniques were considered for the shock tube end-walls. Of these, two methods either failed or were inappropriate for the shock tube simulation. Campbell's [16] method of introducing boundary conditions into the equations of motion was not appropriate for the shock tube problem because the wall pressure is not known. Simulations using immobile particles failed because the momentum of the computational particles was sufficient to enable them to cross over the tube end walls.

Figures 4 and 5 shows density, velocity, temperature and pressure after reflection predicted using the imaginary particle method. The reflective boundary was modeled by placing fifteen extra particles on the opposite side of the tube end. This amount was determined by the number of real particles that came within 2h of the boundary during the simulation. Figure 4 was obtained using M-G viscosity, and Figure 5 using FCT artificial diffusion methods. Flux corrected transport produced nonphysical oscillations behind the reflected shock wave. These oscillations were stable and traveled with the reflected shock

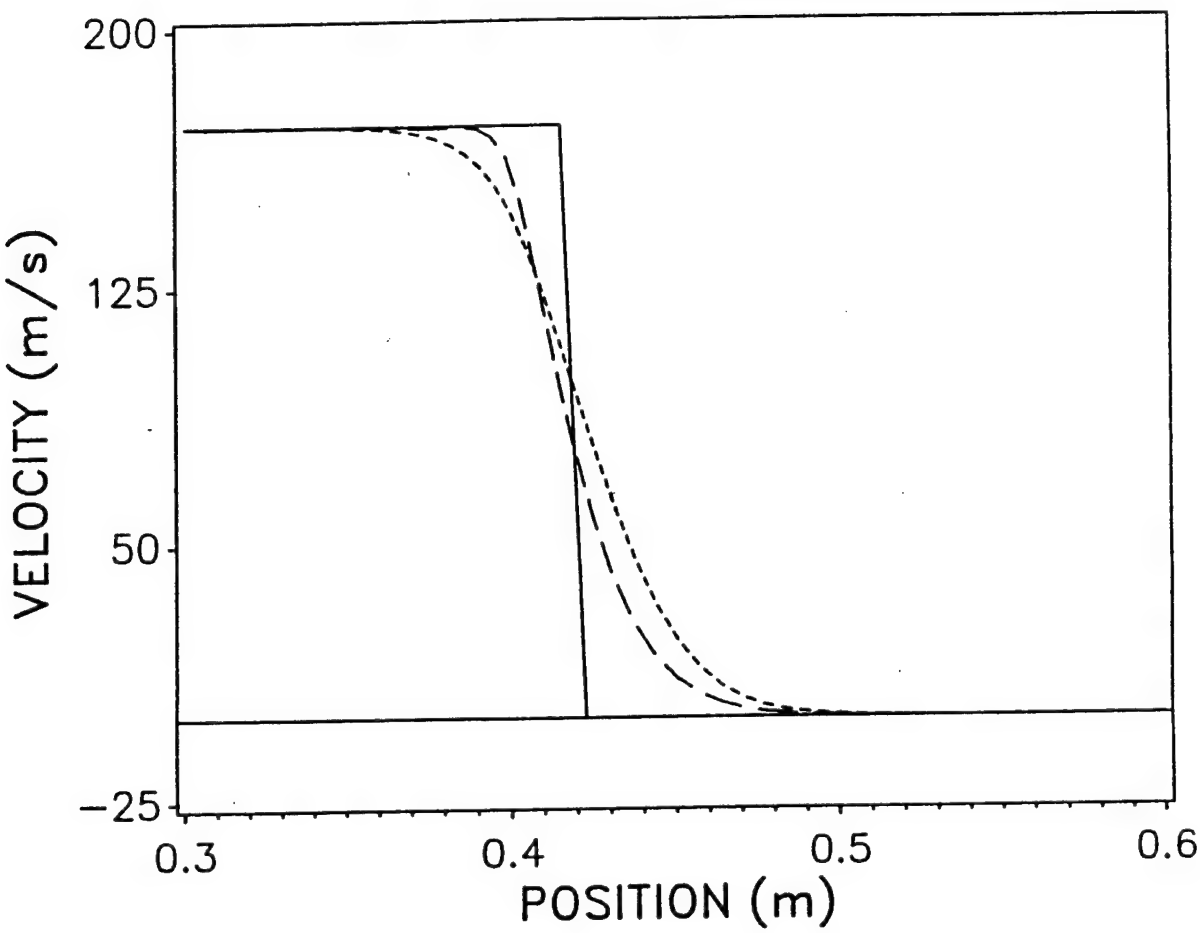

Figure 3: Comparison of pre-reflection shock wave simulations using M-G (fine-dashed line), and FCT (coarse-dashed line) for artificial diffusion. Exact solution is the solid line.

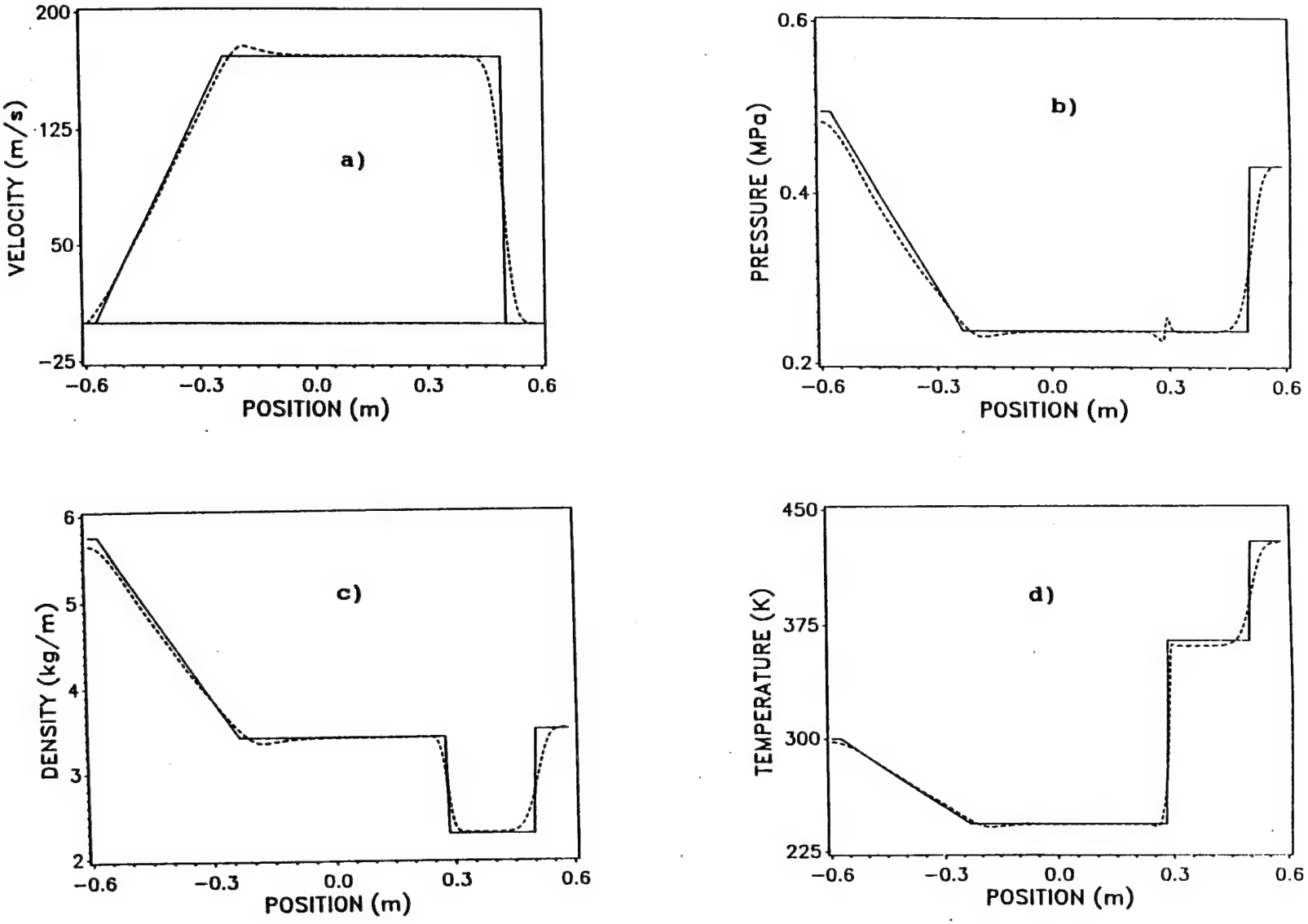

Figure 4: Plots of a) velocity, b) pressure, c) density, and d) temperature 1.65 milliseconds into the simulation, and after reflection. Simulation uses Monaghan-Gingold artificial viscosity (dashed line), and the imaginary particle boundary treatment.

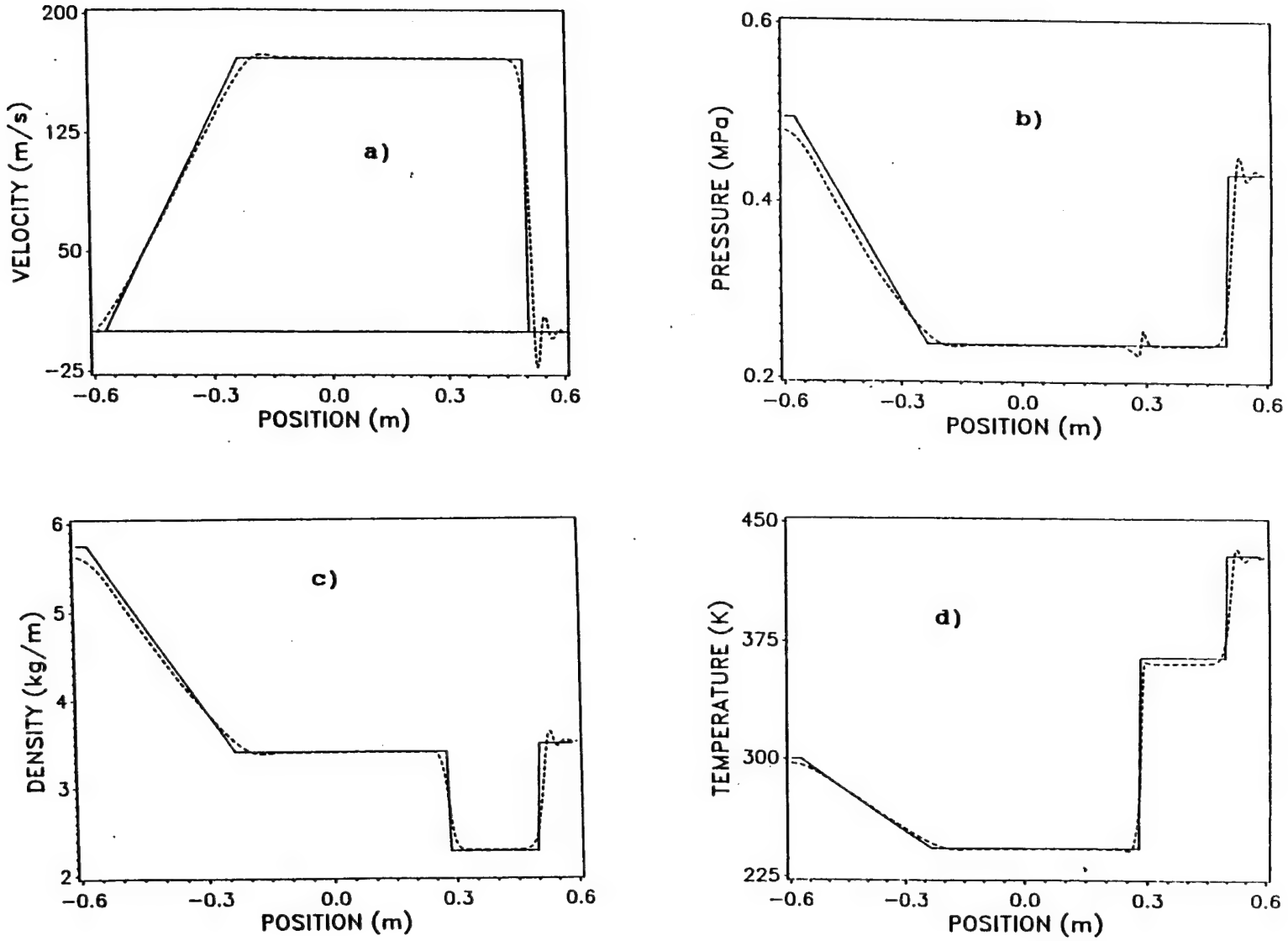

Figure 5: Plots of a) velocity, b) pressure, c) density, and d) temperature 1.65 milliseconds into the simulation, and after reflection. Simulation uses flux corrected transport (dashed line), and the imaginary particle boundary treatment.

wave. Monaghan-Gingold's viscosity produced no oscillations, however the reflected density shock front was more diffused. This is attributed to the reflected shock propagating into a region with higher density. There are more downstream particles within the 2h smoothing length from the shock front than were in the corresponding region for the pre-reflection shock wave. The imaginary particle method compares well with the exact solution.

Both the Lennard-Jones and spring repulsive force schemes produced essentially indistinguishable results. Both schemes experienced particle crossing difficulties. Figures 6 and 7 show density, velocity, temperature, and pressure predictions obtained using the spring force method for M-G and FCT treatments, respectively. Flux corrected transport again shows a tendency to produce nonphysical oscillations on the trailing edge of the reflected shock waves. The velocity plots of both figures show instabilities behind the reflected shock wave. This is due to particles crossing each other (though not the end-wall) near the edge of the applied force. The instabilities eventually damp out as the reflected wave propagates away from the tube wall.

The density, temperature, and pressure plots show a shortcoming of the repulsive force technique; a drop in value along the boundary edge. This is caused by the particles near the tube end missing part of their summation. The spurious pressure and density drops cause an initial velocity toward the tube end. While the repulsive force acts to prevent this initial acceleration, it is does not effect the values of the density or pressure, and they remain underpredicted. An attempt was made to use the alternative conservation of mass equation (Eq. 11), as

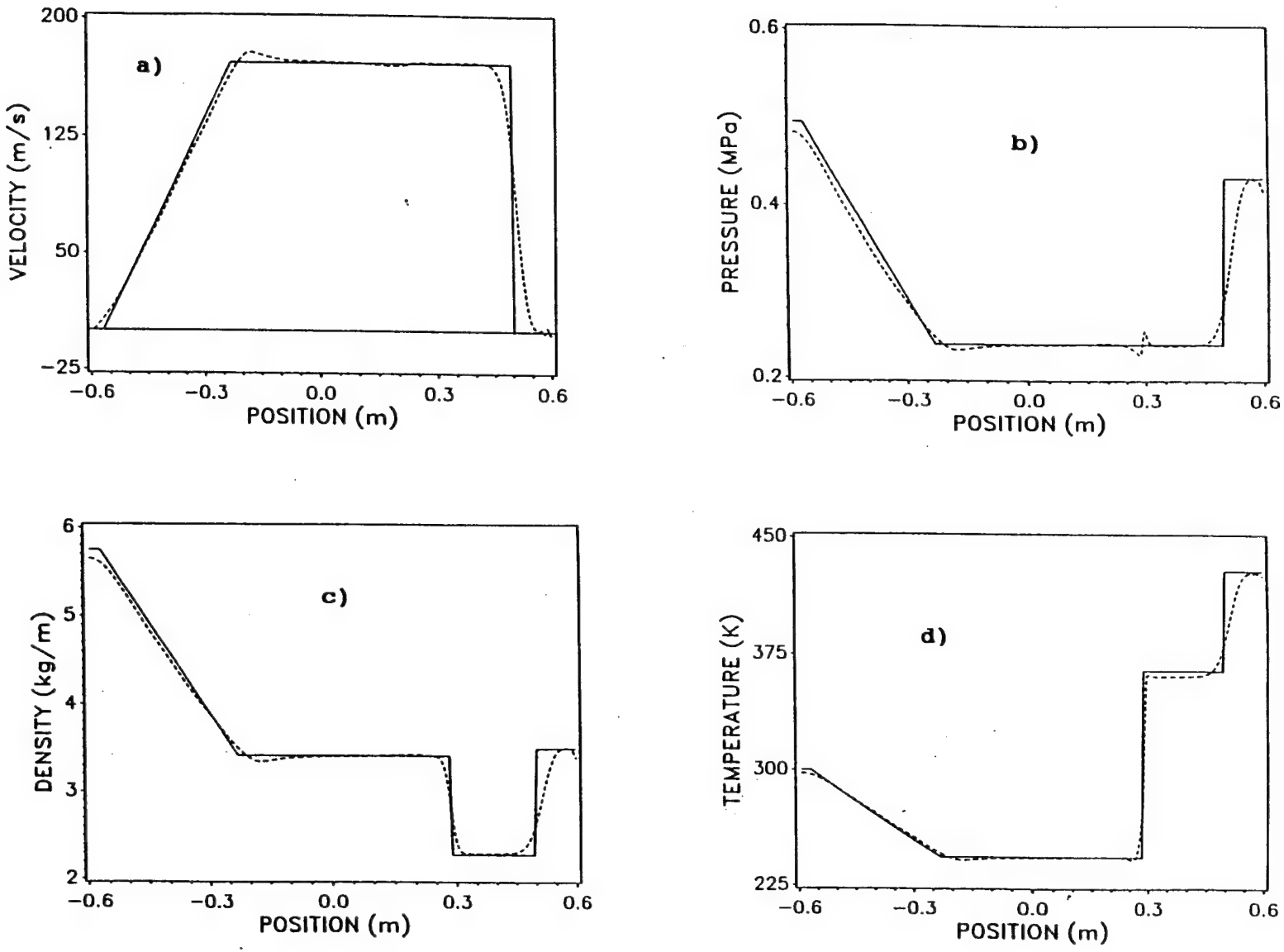

Figure 6: Plots of a) velocity, b) pressure, c) density, and d) temperature 1.65 milliseconds into the simulation, and after reflection. Simulation uses Monaghan-Gingold artificial viscosity (dashed line), and the repulsive force (spring) boundary treatment.

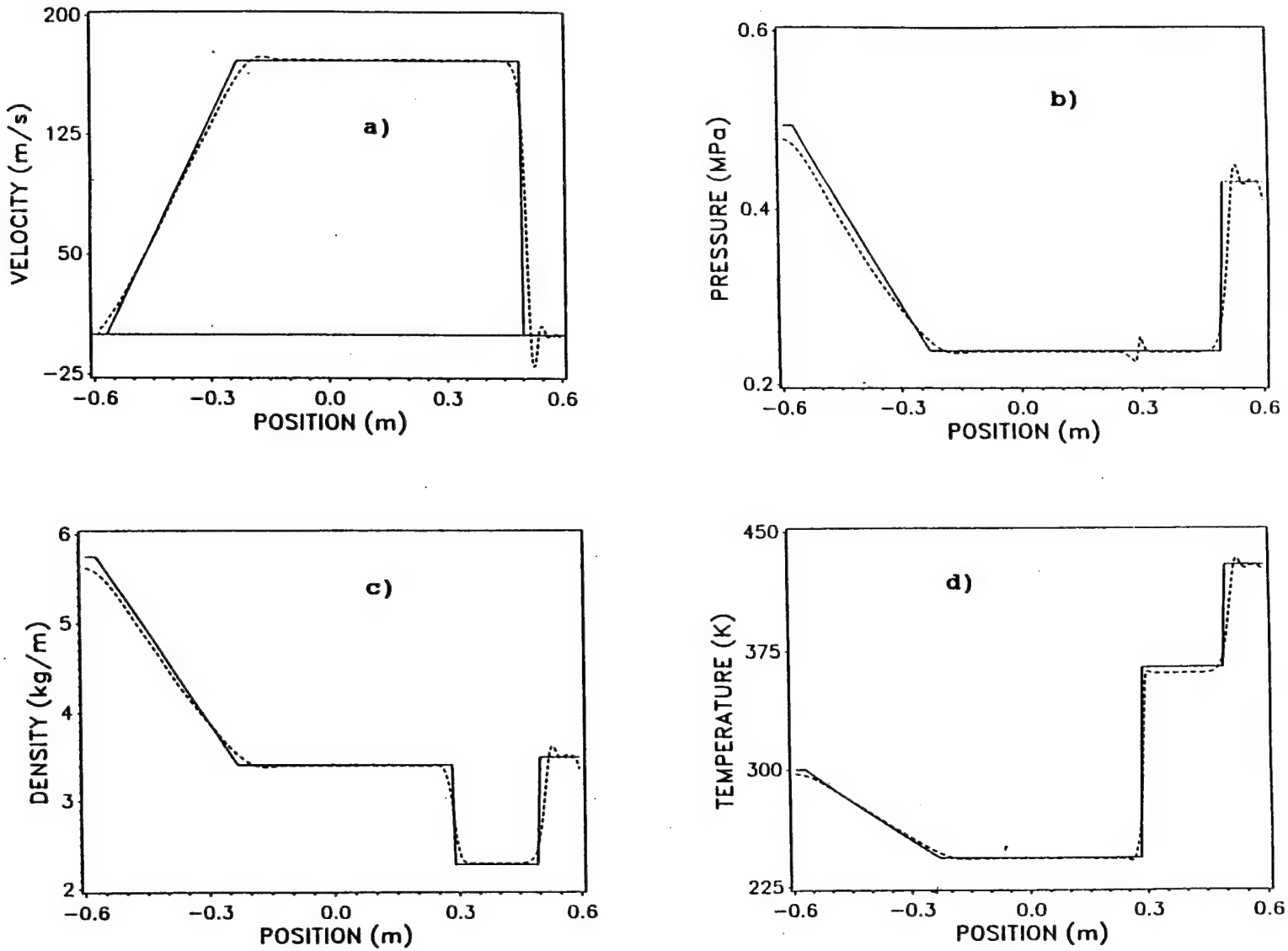

Figure 7: Plots of a) velocity, b) pressure, c) density, and d) temperature 1.65 milliseconds into the simulation, and after reflection. Simulation uses flux corrected transport (dashed line), and the repulsive force (spring) boundary treatment.

this method calculates the density using the velocity divergence instead of particle mass summation. Simulations showed that after the reflection there still remained a drop in the expected value because of the missing parts of the divergence summation.

3.3 Conclusion

Conclusions about the relative performance of SPH simulations of reflected shockwaves using artificial diffusion schemes are somewhat ambiguous. Monaghan and Gingold's viscosity [9] and flux corrected transport [20] have been compared. Though FCT reproduces the sharpest shock fronts, it appears less stable after the reflection and more limited in application than M-G viscosity. However, post-reflection simulations using M-G viscosity produce more heavily smeared shock waves.

Conclusions pertaining to different boundary treatments are less ambiguous. The most accurate simulations of the reflected shock were made using the imaginary particle scheme; although CPU time, memory requirements, and coding complications were greater than for other candidate schemes. Coding techniques can reduce the extra CPU and memory requirements for applications in higher dimensions. The repulsive force technique is the easiest to code and requires less CPU time, however accuracy is sacrificed and particles may cross. Neither the immobile particle technique, nor Campbell's [16] pressure modification boundary technique were suitable for this test case.

Chapter 4: INCOMPRESSIBLE FLOW

4.1 Introduction

The emphasis of the previous chapters was on developing the SPH formalism and applying the method to one-dimensional, compressible, inviscid flow. The object of this chapter is to extend the SPH method to model two-dimensional, viscous, incompressible flow. The test problem used to accomplish this objective are the shear driven cavity, Couette flow, and Stoke's first problem.

4.2 Modifications

The standard SPH technique for solving the equations of motion utilize summations, based on particle locations and a weighting kernel, to determine the density, velocity and internal energy. The pressure is a thermodynamic property generally obtained from the density, internal energy, and an appropriate equation of state.

The governing equations for incompressible viscous flow are:

$$\partial\rho/\partial t\big|_{\text{artificial}} + \nabla\cdot(\rho v) = 0 \tag{28}$$

$$d\rho v/dt = -\nabla\cdot P + \rho\Pi' \tag{29}$$

When modeling incompressible flow, the standard SPH procedure must be modified because density no longer effects pressure through an equation of state. This modification is introduced by using an artificial compressibility formulation.

4.2.1 Artificial compressibility

The basis for the artificial compressibility scheme lies in introducing a time derivative of pressure. This term can be incorporated into an equation of state. The following equation of state for water has been applied by Monaghan [14] for modeling free surface flows:

$$P = B((\rho/\rho_0)^{\Gamma}-1), \tag{30}$$

with $\Gamma = 7.415$. The constant B is simulation specific, and depends on the maximum fluid velocity. In the artificial incompressibility technique, the speed of sound is defined as being very much larger than the maximum possible speed of the bulk flow ($c > 0.1*Vmax$). This puts a limit on the maximum change in the density values. The constant B is used to keep the density changes to within approximately 5% of the original values. In these simulations B was defined as follows:

$$B = (V_{max}/0.1)^2 * \rho_0/\gamma'. \tag{31}$$

Where γ' is the fluid's specific heat ratio. This technique models an incompressible fluid as slightly compressible.

4.2.2 Viscous term

A common requirement for all the previously cited SPH formulations is to include an artificial viscosity component to the dampen the high frequency oscillations inherent to Lagrangian simulation techniques. However, in simulating viscous, recirculating flows of engineering interest, true viscosity must be used.

The viscous term of the Eulerian momentum equation is written as

$$\Pi' = 1/\rho \ \nabla\cdot(\nu'\nabla v). \tag{31}$$

While this can be substituted directly into the SPH formulation, it has been shown [22,23] that the second derivative is extremely sensitive to particle disorder. To avoid this problem in the heat diffusion equation, an integral approximation was used to model the second derivative [22,23]. Because of the direct analogy between heat diffusion and viscous momentum diffusion, this technique has been applied here for the viscous term. Through application of this technique, the viscosity term becomes:

$$\Pi' = -\Sigma m_j * (2\nu'(v_i - v_j)(r_{ij} \cdot \nabla_j W_{ij})) \;/\; (\rho_{ij}(r_{ij}^2 + \eta^2) \qquad (32)$$

where ν' is the kinematic viscosity, and ρ_{ij} is the averaged density.

4.3 Boundary Treatment

Using the results from the previous chapter as a guide, boundaries were simulated using a hybrid scheme involving both immobile particles and repulsive forces. Immobile particles were placed surrounding the required geometry with the boundary particles exerting the repulsive force. The hybrid technique was used to prevent the near boundary density dropoffs intrinsic to the repulsive force treatment while maintaining the ease and minimum CPU time requirements characteristic of the repulsive force technique. Three layers of immobile particles were necessary to provide the correct values for the edge particles. The repulsive force was modeled using the Lennard-Jones type force (Eqn. 26) and was exerted solely by the first layer of immobile particles.

4.4 The Test Problems

The first test problem for the viscous, incompressible formulation was Couette flow. Couette flow is steady viscous flow between two infinitely long parallel plates with the lower plate stationary and the top plate moving at a constant speed. The fully developed solution yields a linear velocity profile. This test problem was used to determine if the viscous boundary conditions were being accurately modeled.

Stoke's first problem was the next test case. This problem involves the transient flow development for a fluid near a suddenly moving infinitely long plate. Results are compared to the exact solution. This problem was used to determine if diffusion is being properly modeled in the transient case, as pressure gradients do not contribute significantly to the fluid motion in this problem.

The third test problem is the classic shear driven cavity flow. With this problem, the moving top of a closed square cavity produces a recirculation pattern in the fluid. A solution was obtained for a Reynolds number ($U_{top}H/\nu$) of 10. Results are compared with solutions obtained from the Eulerian code described by Miller and Schmidt [24]. This test problem tests all three major areas of interest: the boundary conditions, the viscous diffusion, and the artificial compressibility.

In all test problems the transient equations were stepped in time with the same Runge-Kutta scheme described previously. No artificial diffusion has been included in any of the simulations. The test problems were simulated with 676 particles. Of these, 277 particles

were used for the boundaries, and were not independently cycled through the summations.

4.5 Discussion

Figure 8 is a plot of the velocity profile for the Couette flow simulation. This result matches with the expected solution (constant slope). The velocity profile was taken at a time well after the steady state solution was achieved. This indicates that the hybrid boundary condition is accurately modeling the moving surface, and the viscous effects are being properly modeled for the fully developed state.

Figure 9 is a plot of the transient velocity profile for Stoke's first problem. The SPH solution is compared with a similarity solution [25]. Smoothed particle hydrodynamics underpredicts the exact solution by approximately 10 percent for the particle closest to the boundary. Particles further from the boundary show better comparisons with the expected solution. It is expected that the relatively high error for the particle nearest the boundary can be diminished by the addition of more particles near the moving plate.

Figure 10 shows the steady-state streamlines for the particles in the driven cavity flow problem. Figure 11 shows the actual particle locations for the same time (120 seconds). These plots show that SPH reproduces the expected physics of the problem and the particles maintain an essentially equal separation. A noticeable error lies in the upper right corner of the cavity in figure 11. An area depleted of particles form soon after the simulation is started. Figures 12 and 13 show the horizontal and vertical velocity profile for the SPH

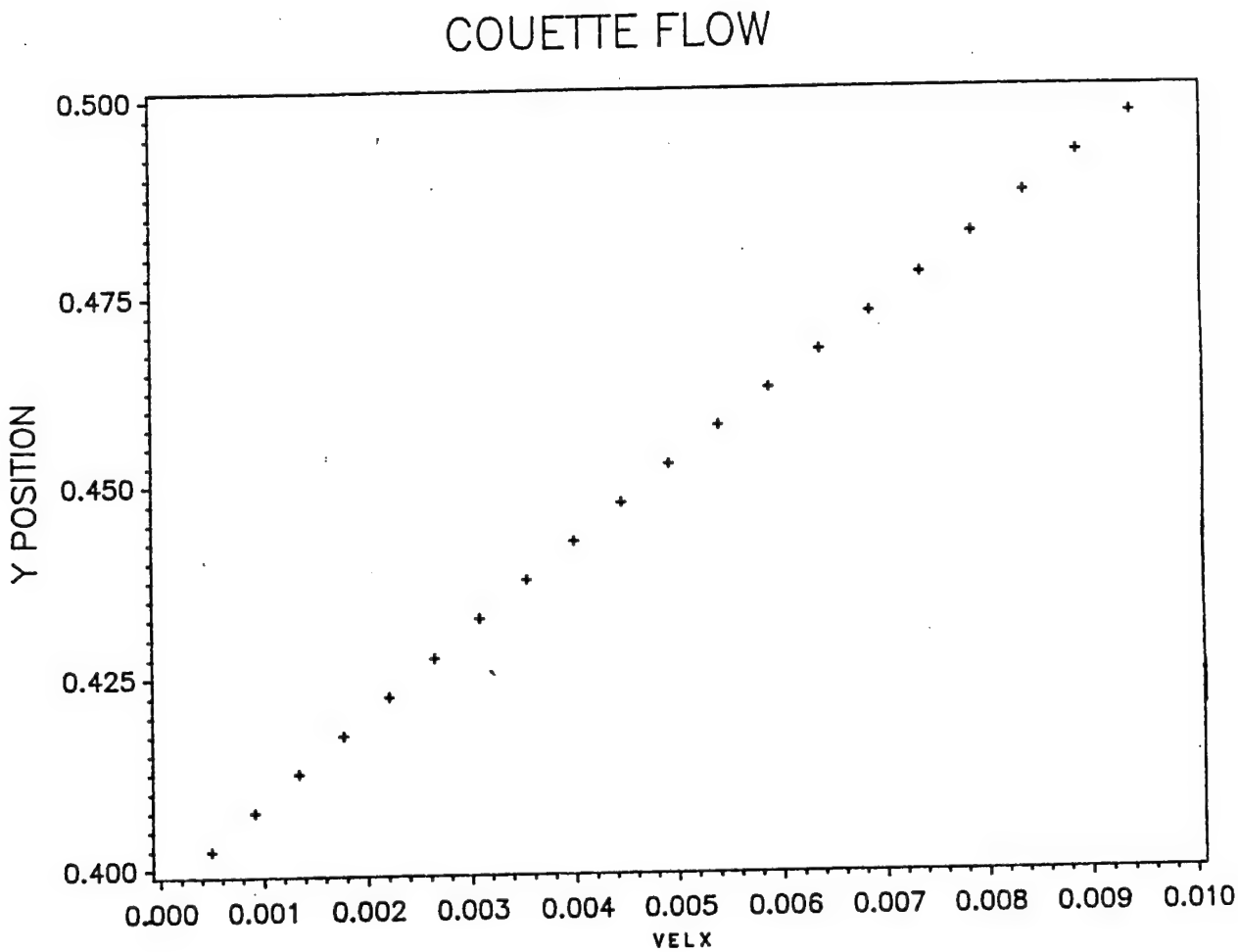

Figure 8: Plot of the fully developed velocity profile for Couette flow.

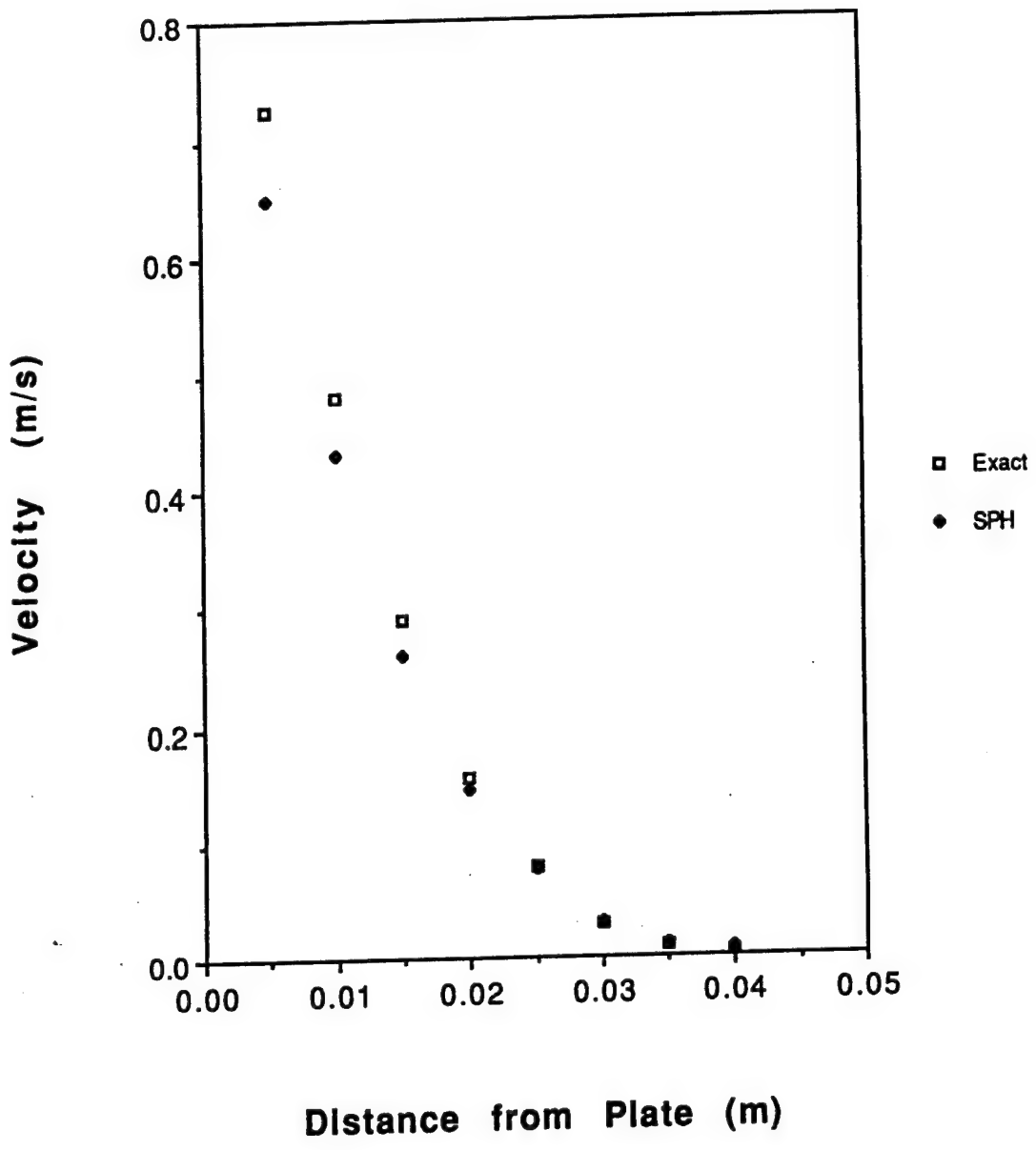

Figure 9: Plot of transient velocity profile for Stoke's first problem at 0.001 seconds (dashed line).

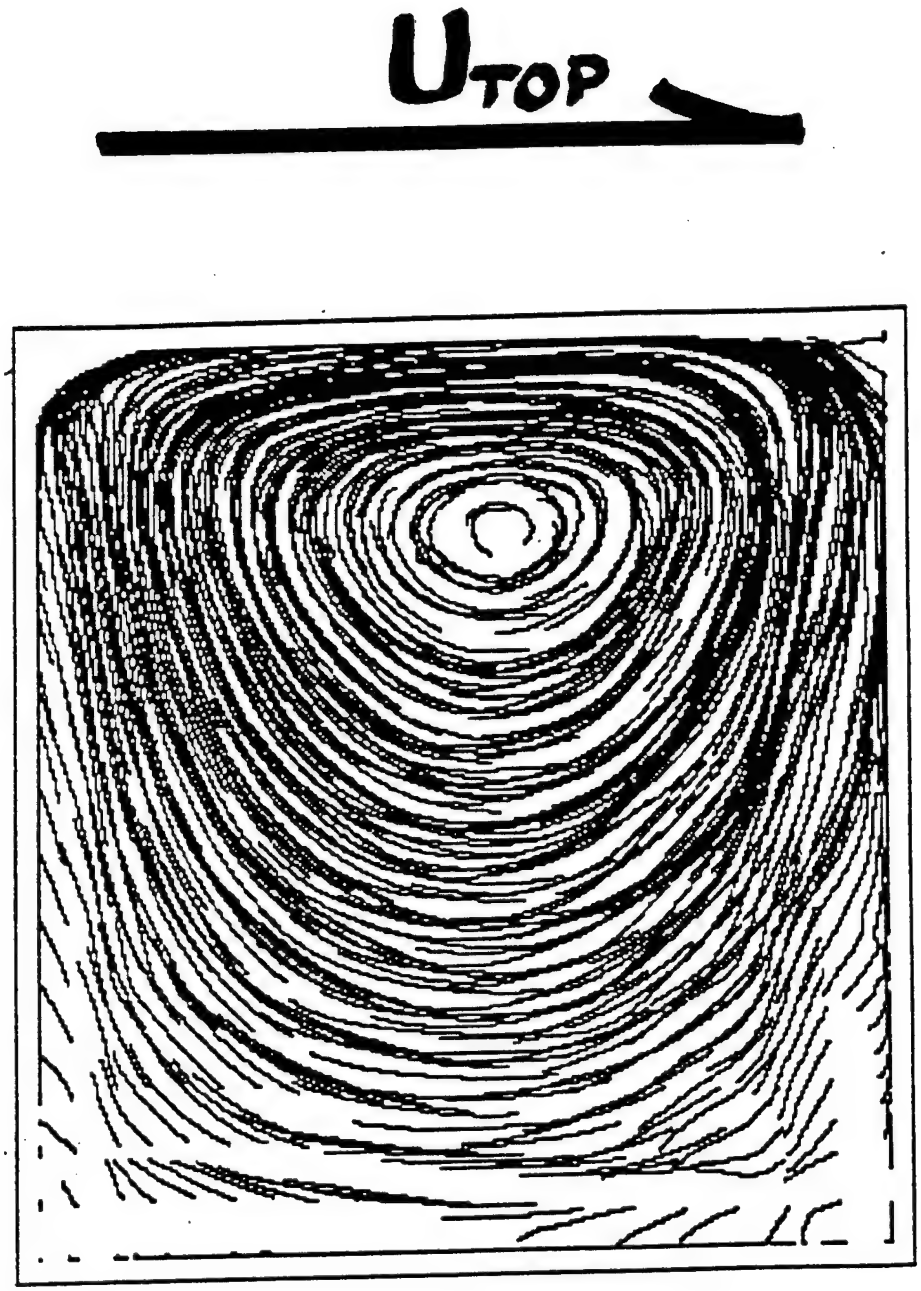

Figure 10: Particle streaklines at 120.0 seconds for a Reynold's number of 10

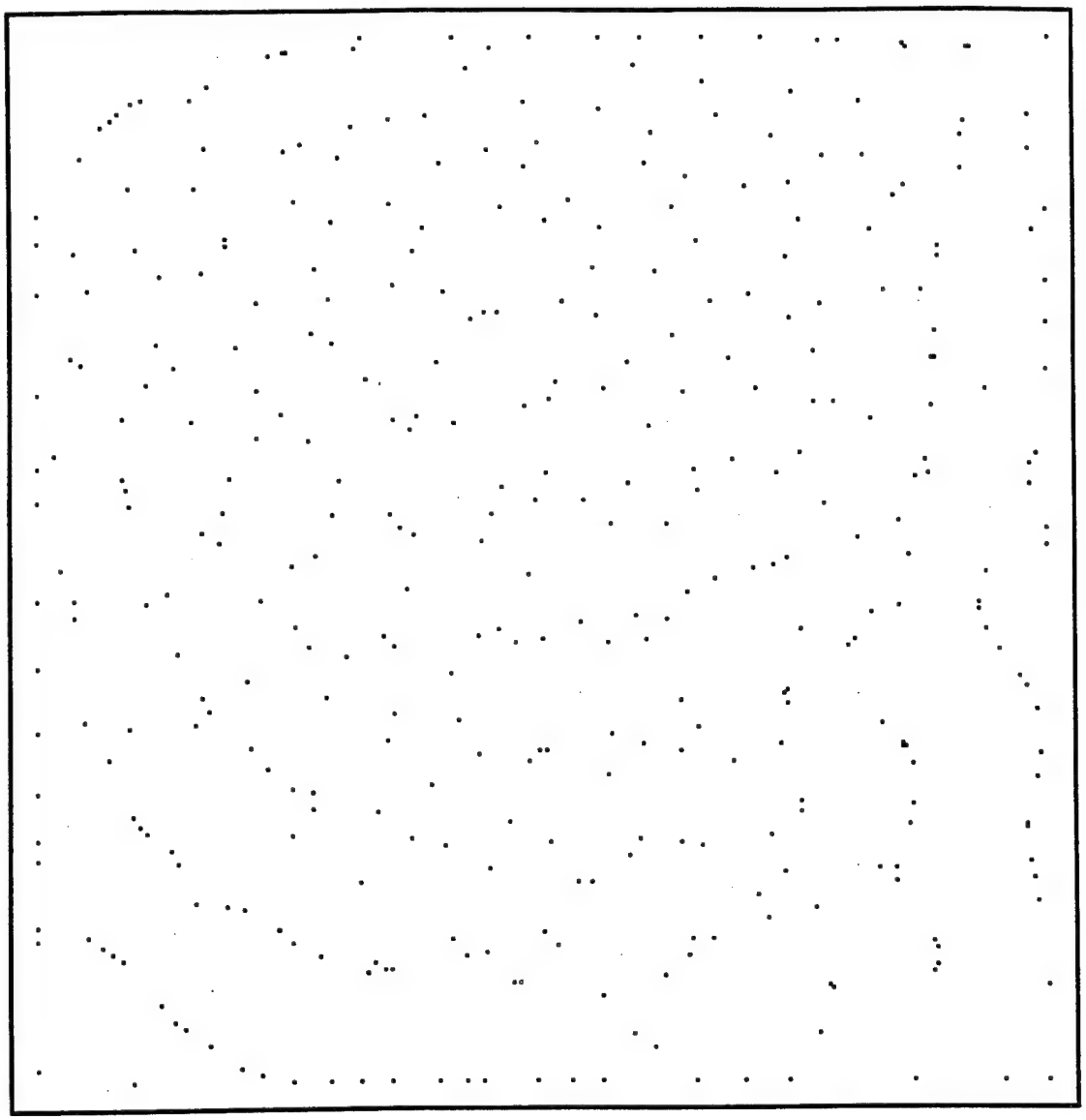

Figure 11: Particle distribution at 120.0 seconds for the driven cavity with a Reynold's number of 10.

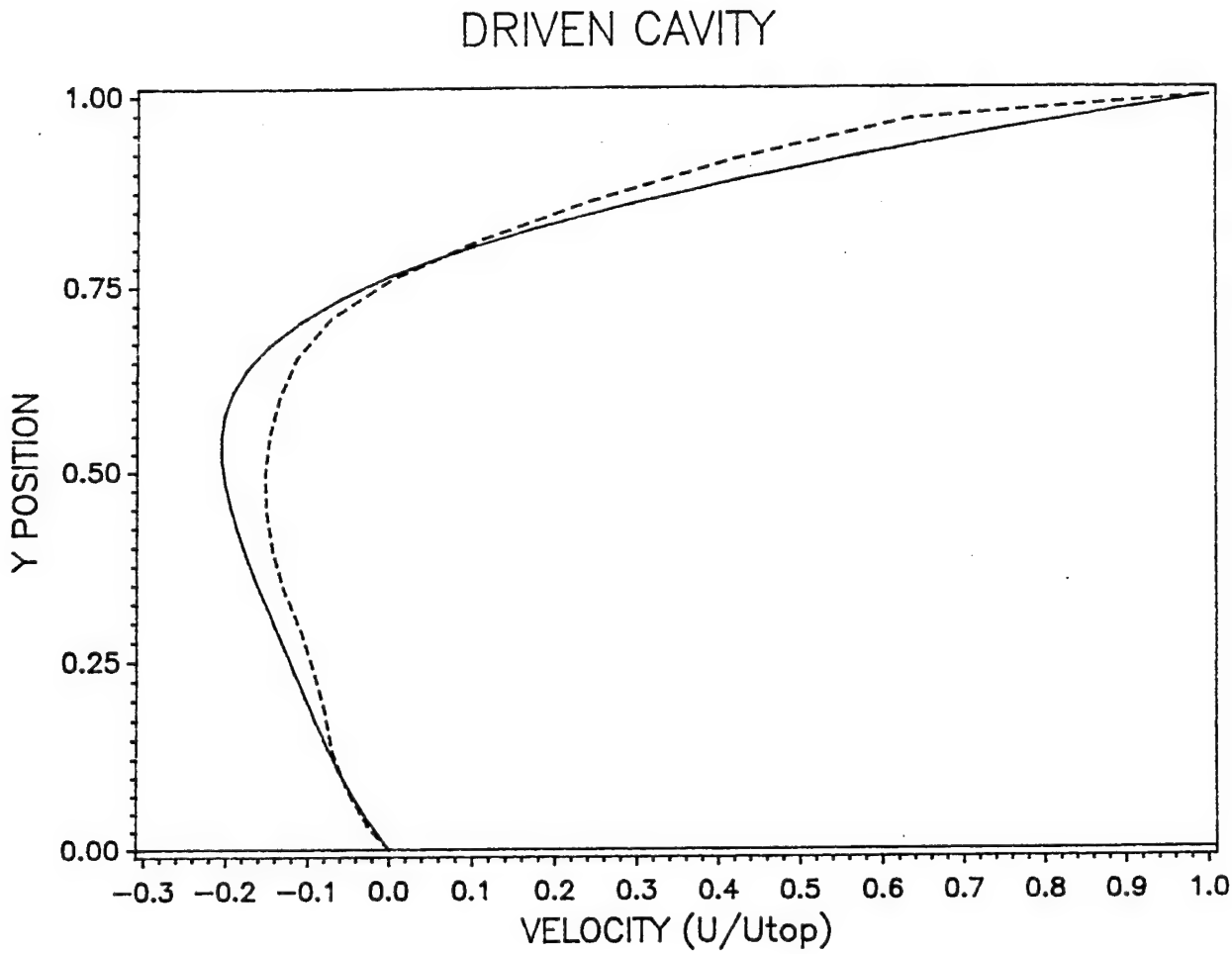

Figure 12: Velocity profile along vertical centerline for the driven cavity with a Reynold's number of 10.

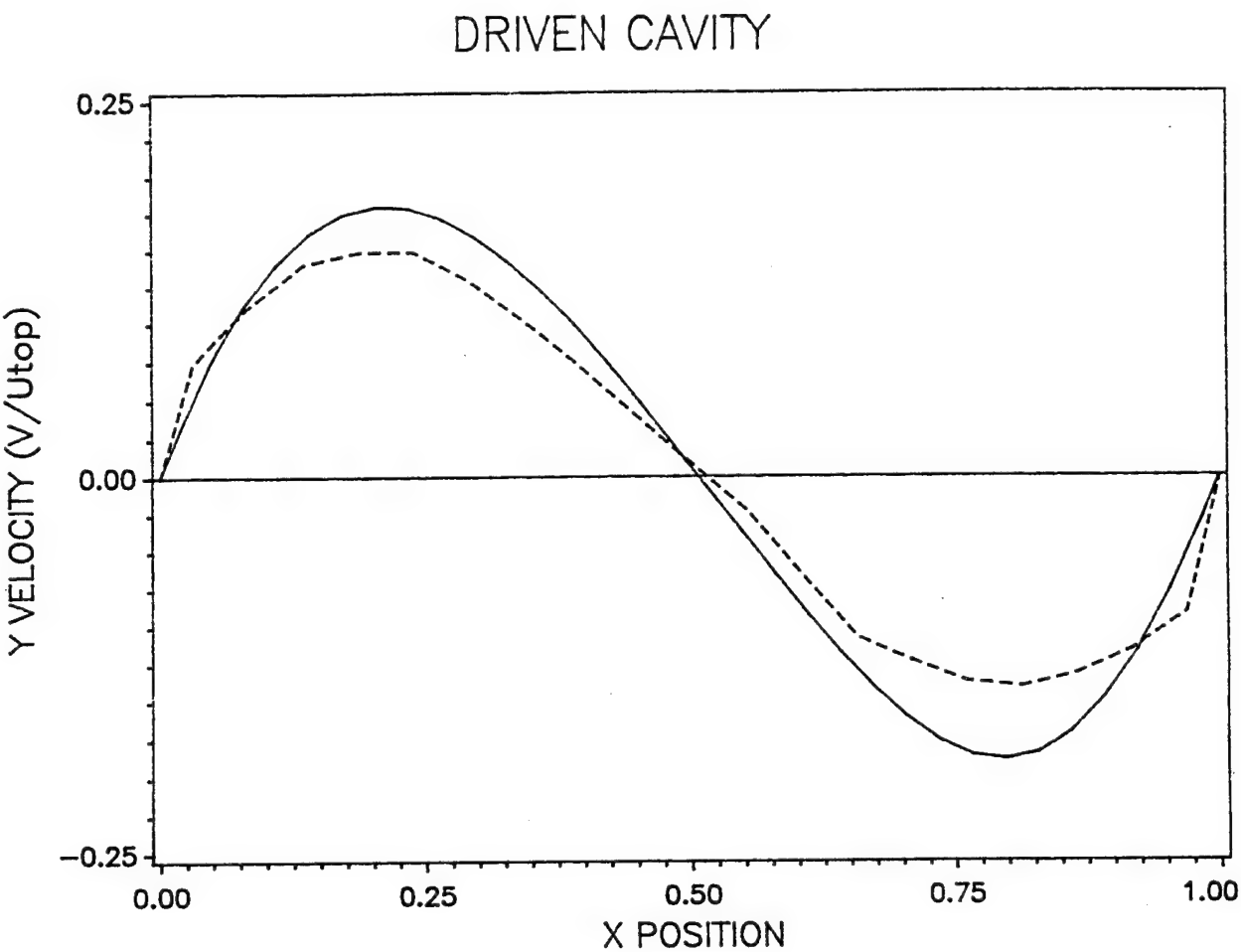

Figure 13: Velocity profile along horizontal centerline for Reynold's number of 10.

simulation, respectively. The SPH solutions (dashed lines), are compared with the Eularian solutions of Miller and Schmidt [24] (solid lines). Since SPH is a gridless technique, interpolation was necessary to determine the velocity profile. Both plots show an underprediction in the velocity values. Because the Couette flow and Stoke's first problem simulations compared well with theory, the discrepancy in the driven cavity simulation is not attributed to the viscous stress or the no-slip boundary condition. Rather, the error is attributed to the occurrence of the particle depletion regions. It is expected that with the addition of more particles the solution will converge closer to the expected result.

4.6 Conclusions

Conclusions regarding the SPH treatment of incompressible, viscous flows are encouraging. Smoothed particle hydrodynamics successfully treats the Couette flow and Stoke's first problem. This indicates that both the viscous stress and the no-slip boundary are being properly modeled. The driven cavity underpredicts the expected solution and the error is attributed to a loss in resolution due to low particle areas.

Chapter 5. CONCLUSIONS/RECOMMENDATIONS

Smoothed particle hydrodynamics has been shown to have the potential to accurately model flows beyond its original astrophysical applications. Boundaries have been implemented successfully through a variety of techniques. The final choice of boundary technique, ultimately lies in the memory and CPU requirements of the user. Flux corrected transport can be introduced into the SPH formulation and it has advantages and disadvantages.

Smoothed particle hydrodynamics has been shown to have great potential in modeling incompressible flow. The artificial compressibility treatment and the introduction of true viscosity reproduce the physics of the test problems, though not to a desirable accuracy in the driven cavity. The area of error has been determined to be a loss of resolution due to too few particles.

Recommendations for further study include: application of the artificial diffusion technique, flux corrected transport, to higher dimensions; finding the optimum technique for introducing viscosity; introducing particles in depleted regions; and extending the technique to modeling multi-fluid flows.

REFERENCES

1) Lucy, L., "A Numerical Approach to Testing the Fission Hypothesis," *Astronomical Journal*, Vol. 82, 1977, pp. 1013-1024.

2) Gingold, R.A., Monaghan, J.J., "Smoothed Particle Hydrodynamics: Theory and Application to Non-spherical Stars," *Monthly Notices of the Royal Astronomical Society*, Vol. 181, 1977, pp. 375-389.

3) Gingold, R.A., Monaghan, J.J., "Binary Fission in Damped Rotating Polytropes," *Monthly Notices of the Royal Astronomical Society*, Vol. 184, 1978, pp. 481-499.

4) Herant, M., Benz, W., "Hydrodynamical Instabilities and Mixing in SN1987A: Two-Dimensional Simulation of the First 3 Months," *Astrophysical Journal*, Vol. 370, 1991, pp. L81-84.

5) Benz, W., Slattery, W.L., Cameron, A.G.W. "The Origin of the Moon and the Single-Impact Hypothesis I," *Icarus*, Vol. 66, 1986, pp. 515-535.

6) Benz, W., Slattery, W.L., Cameron, A.G.W. "The Origin of the Moon and the Single-Impact Hypothesis II," *Icarus*, Vol. 71, 1987, pp. 30-45.

7) Benz, W., Cameron, A.G.W., Melosh, H.J., "The Origin of the Moon and the Single-Impact Hypothesis III," *Icarus*, Vol. 81, 1989, pp. 113-131.

8) Libersky, L.D., Petschek, A.G., "Smooth Particle Hydrodynamics With Strength of Materials," *Advances in the Free-Lagrange Method*, Vol. 395, Springer-Verlag, Berlin, 1991, pp. 248-257.

9) Monaghan J.J., Gingold, R.A., "Shock Simulation by the Particle Method SPH," *Journal of Computational Physics*, Vol. 52, 1983, pp. 374-389.

10) Lattanzio, J.C., Monaghan, J.J., Pongracic, H., Schwarz, M.P., "Controlling Penetration," *SIAM Journal on Scientific and Statistical Computing*, Vol. 7, pp. 591-598.

11) Haddad, B., Clausset, F., Combes, F., "Vectorising the Smooth Particle Hydrodynamics," *Journal of Computational Physics*, Vol. 97, 1991, pp. 103-126.

12) Henneken, E.A.C., Icke, V., "SPH Faces Emery's Jump," *Computer Physics Communications*, Vol. 74, 1993, pp. 239-246.

13) Nagasawa, M., Kuwahara, K., "Smoothed Particle Simulations of the Pyroclastic Flow," *International Journal of Modern Physics B*, Vol. 7, Nos. 9&10, 1993, pp. 1980-1995.

14) Monaghan, J.J., "Simulation Free Surface Flows with SPH", preprint, Department of Mathematics, Monash University, 1992.

15) Monaghan, J.J., "An Introduction to SPH," *Computer Physics Communications*, Vol. 48, 1988, pp. 89-96.

16) Campbell, P.M., "Some New Algorithms for Boundary Value Problems in SPH," Mission Research Corporation, 1988.

17) Monaghan, J.J., "Particle Methods for Hydrodynamics," *Computer Physics Reports*, Vol. 3, No. 2, 1985, pp. 71-124.

18) Rhodes, C.E., "A Fast Algorithm for Calculating Particle Interactions," *Computer Physics Communications*, Vol. 70, No.3, 1992, pp. 478-482.

19) Monaghan, J.J., Lattanzio, J.C., "A Refined Particle Method for Astrophysical Problems," *Astronomy and Astrophysics*, Vol. 149, pp. 135-143.

20) Boris, J.P., Book, D.L., "Flux-Corrected Transport I:SHASTA, A Fluid Transport Algorithm That Works," *Journal of Computational Physics*, Vol. 11, 1973, pp. 38-69.

21) Book, D.L., Boris, J.P., Hain, K., "Flux-Corrected Transport II:Generalizations of the Method," *Journal of Computational Physics*, Vol. 18, 1975, pp. 248-283.

22) Brookshaw, L., "The Stability of Binary Systems and Rotating Stars," PhD Thesis, Monash University. 1986.

23) Monaghan, J.J., "Smoothed Particle Hydrodynamics," *Annual Review of Astronomy and Astrophysics*, Vol. 30, 1992, pp.534-574.

24) Miller, T.F., Schmidt, F.W., "Use of a Pressure-Weighted Interpolation Method for the Solution of the Incompressible Navier-Stokes Equations on a Nonstaggered Grid System," *Numerical Heat Transfer*, Vol. 14, 1988, pp. 213-233.

25) Schlichting, H. Boundary-Layer Theory. McGraw Hill, 6th ed. 1968, pp. 82-83.